Iran J Nucl Med. 2025;33(2):116-124 [Serial No. 65]

*Homepage:* https://irjnm.tums.ac.ir/

*ORIGINAL RESEARCH ARTICLE*

# Estimation of human absorbed dose for [$^{113m}$In]In-AMBA using animal experimental data and Monte Carlo simulation

**Samaneh Zolghadri, Arezou Karimian, Mohsen Mehrabi, Hassan Yousefnia**

*Radiation Application Research School, Nuclear Science and Technology Research Institute, Tehran, Iran*

**ARTICLE INFO**

***Article History:***
Received: 27 January 2025
Revised: 31 May 2025
Accepted: 03 June 2025
Published Online: 20 June 2025

***Keyword:***
[$^{113m}$In]In-AMBA
Monte Carlo
ORNL
MIRD
S-value

*Corresponding Author:
Dr. Hassan Yousefnia
Address: Radiation Application Research School, Nuclear Science and Technology Research Institute, Tehran, Iran
Email: hyousefnia@aeoi.org.ir

**ABSTRACT**

**Introduction:** Gastrin-releasing peptide receptors (GRPRs) are overexpressed in a wide range of malignancies, making them attractive targets for molecular imaging and targeted therapy. The bombesin analog DO3A-CH2CO-G-[4-aminobenzoyl]-QWAVGHLM-NH2 (AMBA), has demonstrated promising potential in both diagnostic and therapeutic applications by selectively binding to GRPRs. This study aimed to estimate the absorbed dose of [$^{113m}$In]In-AMBA, based on preclinical biodistribution data and Monte Carlo simulations.

**Methods:** AMBA peptide was radiolabeled with $^{113m}$In prepared from an in-house developed $^{113}$Sn/$^{113m}$In generator. Biodistribution studies were performed in rats at multiple time points following the injection of [$^{113m}$In]In-AMBA. The accumulated activity in each rat organ was extrapolated to human organ. Finally, the absorbed doses in human organs were estimated by applying the Monte Carlo N-Particle (MCNP) software in Oak Ridge National Laboratory (ORNL) phantom using the Medical Internal Radiation Dose (MIRD) method.

**Results:** The radiochemical purity (RCP) of [$^{113m}$In]In-AMBA exceeded 98% (HPLC). Biodistribution studies demonstrated high cumulation of activity in the GRPR-expressing organs and kidneys. The highest absorbed doses were observed in the pancreas (0.0044 mGy/MBq), and kidneys (0.0018 mGy/MBq), respectively. In contrast, non-target organs exhibited minimal uptake and rapid clearance from the animal body results in minimal absorbed dose in non-target organs (≤ 0.001 mGy/MBq).

**Conclusion:** This study demonstrates that [$^{113m}$In]In-AMBA is a safe and promising SPECT imaging agent for the detection of GRPR-positive tumors. While current findings support the safety and potential of [$^{113m}$In]In-AMBA as a GRPR-targeted SPECT agent, further validation in tumor-bearing animal models and early-phase clinical studies is required for clinical translation.

Use your device to scan and read the article online

How to cite this article: Zolghadri S, Karimian A, Mehrabi M, Yousefnia H. Estimation of human absorbed dose for [$^{113m}$In]In-AMBA using animal experimental data and Monte Carlo simulation. Iran J Nucl Med. 2025;33(2):116-124.

https://doi.org/10.22034/irjnm.2025.129999.1674

## INTRODUCTION

GRPRs are overexpressed in various malignancies, including breast, prostate, small cell lung, Gastrointestinal, uterine, ovarian, pancreatic, and some head and neck cancers [1-4]. These receptors play an important role in the growth, division, and metastasis of cancer cells by activating specific pathways. Overexpression of GRPR makes this receptor a valuable molecular target allowing for non-invasive and targeted detection of tumors [5]. Continued research on GRPRs holds promise for the development of innovative diagnostic and therapeutic strategies aimed at improving cancer detection and treatment outcomes [6].

Bombesin (BBN), a 14-amino acid peptide, and its analogs have gained attention in molecular imaging and targeted therapies due to their binding to GRPR [6, 7]. AMBA is a rationally designed analog of the natural BBN peptide, engineered to enhance pharmacokinetic properties and GRPR-binding affinity. AMBA uses a modified glycyl-4-aminobenzoic acid linker that is more stable and effective than the linkers used in BBN. In addition, it shows strong binding to both BB1 and BB2 receptors for tumor targeting.

AMBA can be radiolabeled with a variety of radionuclides to use diagnosis and therapy [7, 8]. Recent studies have shown that labeling AMBA with radionuclides such as $^{177}$Lu, $^{68}$Ga, $^{67}$Ga, and $^{111}$In has resulted in successful outcomes in diagnosis and treatment [7, 9, 10]. Among these, $^{111}$In-AMBA has shown particularly favorable pharmacokinetics and bioavailability in human tumor models. It offers enhanced receptor stability and greater tumor uptake compared to other analogs such as $^{67}$Ga-AMBA and $^{177}$Lu-AMBA. Additionally, its effectiveness for precise imaging with micro-SPECT/computed tomography (CT) and selectivity for cancer cells reduce side effects in healthy tissues, making it an ideal candidate for diagnostic applications [11].

Therefore, the focus on indium-based radionuclides with this peptide has increased due to the challenges faced by $^{99m}$Tc in SPECT imaging, primarily its shortage of parent radionuclide $^{99}$Mo. The complex chemistry required for $^{99m}$Tc labeling, lacking specific functional groups, has shifted research towards alternative radionuclides with similar half-lives and simpler labeling chemistry for compounds like AMBA, an engineered BBN analog [12].

Recent studies have explored a variety of GRPR-targeted radioligands, including [$^{111}$In]In-AMBA, $^{68}$Ga-AMBA, and $^{177}$Lu-AMBA, showing promising imaging and therapeutic capabilities [9-11]. However, challenges such as the short half-life of $^{68}$Ga, complex labeling chemistry of $^{99m}$Tc, and high radiation burden of $^{177}$Lu limit their widespread clinical application [12]. In this context, [$^{113m}$In] emerges as a practical alternative, offering generator-based availability and favorable imaging characteristics, yet remains underexplored in preclinical GRPR-targeted studies.

$^{113m}$In is a suitable radionuclide for SPECT imaging due to its γ-ray emission of 391.7 keV (64.2%), short physical half-life (1.66 h), and it does not emit β-particles. This radionuclide is available as a $^{113}$Sn/$^{113m}$In generator. Carrier-free $^{113m}$In has also been reported to be successful in imaging various organs including the brain, lungs, and other soft tissues [13-14].

Preclinical dosimetry not only provides a basis for assessing the safety and efficacy of radiopharmaceuticals but also provides a path for prediction and optimization in later clinical phases. This process greatly contributes to reducing errors and increasing success in nuclear medicine. Preclinical dosimetry allows the modeling of drug behavior under different conditions and ensures compliance with global standards. Accurate dose determination in the preclinical stages is a prerequisite for regulatory agencies such as the U.S. Food and Drug Administration (FDA) and Emergency Medical Assistance (EANM) to approve radiopharmaceuticals [15]. Hence, prior to employing the [$^{113m}$In]In-AMBA as a new agent radiopharmaceutical in clinical settings, it is crucial to assess the organ-specific accumulated activity and absorbed dose [16].

The MIRD methodology is a well-established framework for estimating radiation doses in human tissues based on radiopharmaceutical distribution data [17] and a technique was introduced to extrapolate activity accumulation from animal studies to humans [16]. A central parameter in internal dosimetry is the Specific Absorbed Fraction (SAF), which quantifies the fraction of emitted energy from a source organ that is absorbed by a target organ. SAFs are essential for calculating organ-specific dose rates and evaluating radiation exposure profiles [18]. To estimate internal radiation doses accurately, SAF values must be determined, which can be achieved using models like the ORNL phantom and simulation tools such as MCNP codes [19-21]. This study aimed to estimate the absorbed dose associated with the novel SPECT imaging agent [$^{113m}$In]In-AMBA for potential use in diagnosing GRPR-expressing tumors in clinical settings. Using

the MIRD framework and Monte Carlo simulations, SAFs and S-values were determined for various source and target organs for the $^{113m}$In radionuclide. These values were then used to determine organ-specific absorbed doses in humans based on preclinical biodistribution data, thereby supporting the feasibility of [$^{113m}$In]In-AMBA as a diagnostic radiopharmaceutical.

## METHODS

### *Preparation and quality control of [$^{113m}$In]InCl$_3$*

The $^{113}$Sn/$^{113m}$In generator was produced by natural indium which was irradiated in a 30 MeV cyclotron. The irradiated target was loaded onto a zirconium chloride column. [$^{113m}$In]InCl$_3$ was eluted with 0.05 M HCl and its radionuclide, chemical, and radiochemical purity (RCP) were investigated using gamma spectrometry, inductively coupled plasma mass spectrometry (ICP-MS), and radio thin layer chromatography (RTLC) methods, respectively.

### *Preparation, quality control and biodistribution studies of [$^{113m}$In]In-AMBA*

For preparation of the radiolabeled compound, AMBA peptide (30 µg) was added to a vial containing [$^{113m}$In]InCl$_3$, the reaction pH was adjusted to 3.5, and incubated at 95 °C for 10 min. Finally, the RCP was assessed using high-performance liquid chromatography (HPLC) and RTLC methods. Ammonium acetate: methanol was considered as the mobile phase and Whatman paper was used as stationary phase.

For biodistribution studies, [$^{113m}$In] In-AMBA (200 µL; 7.4 MBq) was injected into rats via the tail veins and the biodistribution of the radiolabeled peptide was evaluated in various organs at different time intervals (30, 60, and 120 min). After weighing and measuring the tissues, the percentage of injected dose per gram of tissue (%ID/g) was calculated.

To calculate the cumulated activity (Ã) for each source organ in mice, a two-phase hybrid method was applied, as described in previous dosimetry studies [22]. In the first phase, biodistribution data were collected at four time points: 0, 30, 60, and 120 min post-injection. These data were corrected for physical decay back to the time of injection and normalized to the administered activity. The area under the time–activity curve from 0 to 120 minutes was estimated using the trapezoidal rule, assuming zero activity at time zero for all organs except blood, for which non-zero initial activity was considered. In the second phase, to estimate the remaining activity beyond 120 min, a monoexponential decay function was fitted using the last measured activity (at 120 min) and the known physical decay constant of $^{113m}$In.

The total cumulated activity was obtained by summing the trapezoidal area and the extrapolated tail. All calculations were performed using Microsoft Excel. Although the effective decay constant ideally accounts for both biological and physical elimination, it could not be reliably determined due to the limited post-120 min data. Furthermore, since the biological clearance of [$^{113m}$In]In-AMBA is known to be rapid, the use of only the physical decay constant for extrapolation provides a conservative estimate. This approach may slightly overestimate the tail activity but helps to avoid underestimation of the absorbed dose.

### *S-value calculations*

Between 1970 and 1980, ORNL developed practical dosimetry applications based on the MIRD schema. In 1987, Cristy and Eckerman introduced the ORNL phantom (Figure 1), an age-specific mathematical model of the human body constructed using simplified geometric shapes such as elliptical cylinders and cones. The phantom contains various organs and tissues, including the bladder, respiratory tract, colon, salivary glands, kidneys, head, and brain, whose mass densities and compositions are from publications of the International Commission on Radiological Protection (ICRP) and the International Committee on Radiation Units and Measurements (ICRU) [23].

MCNP is used to simulate the transport of particles such as photons and electrons within organs, which allows the calculation of SAFs. The software uses different methods to calculate the absorbed dose, such as F6 (calculates absorbed dose based on energy deposition) , F4 (converts photon flux into absorbed dose), and F8 (calculates energy deposited by secondary particles) [22, 24]. In this research, SAFs and S-values were calculated using MCNPX for the ORNL adult male phantom. The calculation of SAFs was performed using the MCNPX Version 2.6.0 Monte Carlo simulation code, in conjunction with the adult male phantom developed. The phantom was implemented in a three-dimensional Cartesian coordinate system via the Visual Editor (VISD Version X_22S). Source organs, including blood, lungs, liver, kidneys, intestines, stomach, heart, brain, skin, muscles, and bones, were defined geometrically, and the radionuclide ($^{113m}$In) was assumed to be uniformly distributed within each source volume. To ensure accurate decay modeling, photon energies and emission probabilities of $^{113m}$In were extracted from the

JANIS-4.0 nuclear structure database, and incorporated into the simulation input deck.

Particle transport was simulated in photon-only mode (P) based on the kerma approximation, with electron energy assumed to be locally absorbed. The F6 tally was utilized to compute absorbed dose per unit mass (MeV/g), as it provides high precision and is recommended for internal photon dose estimation in MIRD-based studies. For each source-target organ pair, $10^6$ particle histories were simulated, and the relative statistical error for each result was kept below 5%, ensuring high confidence in SAF values. The simulation geometry was optimized to prevent cell overlap and particle loss, based on prior phantom validation protocols.

To ensure validity, selected SAF values were compared with those reported in OLINDA/EXM 2.0 and prior Monte Carlo studies. Differences were generally within 5%, supporting the reliability of the implemented MCNPX framework. All calculated SAF values were subsequently applied to derive S-values using organ mass definitions consistent with ICRP Publication 89 and ICRU Report 46, ensuring anatomical accuracy in line with international standards. The use of Monte Carlo simulation via MCNPX 2.6.0 was selected over standard software packages such as OLINDA/EXM due to its higher flexibility, geometry customization, and accuracy in modeling particle transport, especially for radionuclides with complex biodistribution. This approach has been previously recommended for internal dosimetry in various studies [25-29].

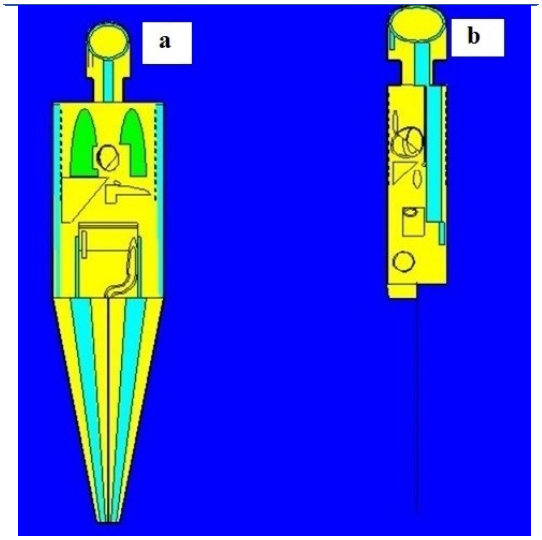


**Figure 1.** The ORNL phantom is depicted in two views: Coronal (a) and Sagittal (b)

### *Accumulated activities of human organs*

To estimate the absorbed dose in humans Eq. 1 was applied to extrapolate the cumulative activity observed in animal models to human models.

$$\bar{A}_{\text{Human organ}} = \bar{A}_{\text{Animal organ}} \times \frac{\text{Organ mass}_{\text{Human}}/\text{Body mass}_{\text{Human}}}{\text{Organ mass}_{\text{Animal}}/\text{Body mass}_{\text{Animal}}} \quad (1)$$

The cumulative activity in the source organ, denoted as $\tilde{A}$, was calculated using (Eq. 2).

$$\tilde{A} = \int_0^{\infty} A(t)dt \quad (2)$$

The activity of each organ at a specific time t, represented as A(t), was analyzed. The cumulative activity in each animal source organ was determined by plotting the percentage of the injected dose as a function of time and calculating the area under the resulting time–activity curve. To extend the curve to infinity, a single exponential fit was applied to the tails of the curves using the physical decay constant of $^{113m}$In. For extrapolation to humans, the average weights of the organs in a standard human model were used [18].

### *Human absorbed dose*

The absorbed dose for each human organ was calculated using the MIRD method, as shown in Eq. 3.

$$D(r_k) = \Sigma_h \tilde{A}_h S(r_k \leftarrow r_h) \quad (3)$$

In this equation, $\tilde{D}(r_k)$ represents the absorbed dose in the organ, and $\tilde{A}_h$denotes the accumulated activity in the source organs. The factor $S(r_k \leftarrow r_h)$ depends on the physical decay properties of the radionuclides, the size of the organs, and the range of the emitted radiation [30].

For each target organ, the absorbed dose was calculated by summing contributions from all source organs with measured activity, including both self-irradiation and cross-irradiation terms, in accordance with the MIRD schema. S-values were obtained from MCNPX simulations based on the ORNL adult male phantom.

## RESULTS

### *Preparation and quality control of [$^{113m}$In]$InCl_3$*

[$^{113m}$In]$InCl_3$ with radionuclide purity >99.99% was used for labeling step. The impurity of $^{113}$Sn in the final solution was 0.0005% which is less than the European Pharmacopoeia limit. Metal ions impurities such as copper, tin, zirconium, zinc,

and iron were < 1 ppm, and the RCP of the [$^{113m}$In]$InCl_3$ solution was more than 99%.

### *Preparation, quality control, and biodistribution studies of [$^{113m}$In]In-AMBA*

[$^{113m}$In]In-AMBA was prepared with 30 µg of AMBA in pH ≈ 3.5, and incubation time 10 min and reaction temperature of 95 °C. The RCP of the final complex was > 98%, (Figure 2). The biodistribution of the radiolabeled compound was assessed in various organs at 30-, 60-, and 120-min post-injection. Non-decay-corrected time-activity curves for [$^{113m}$In]In-AMBA are shown in Figure 3. The highest residual activity was observed in the pancreas, a known GRPR-expressing organ. The kidneys showed the second highest accumulation site due to the hydrophilic nature of the peptides and their rapid clearance through urine tract.

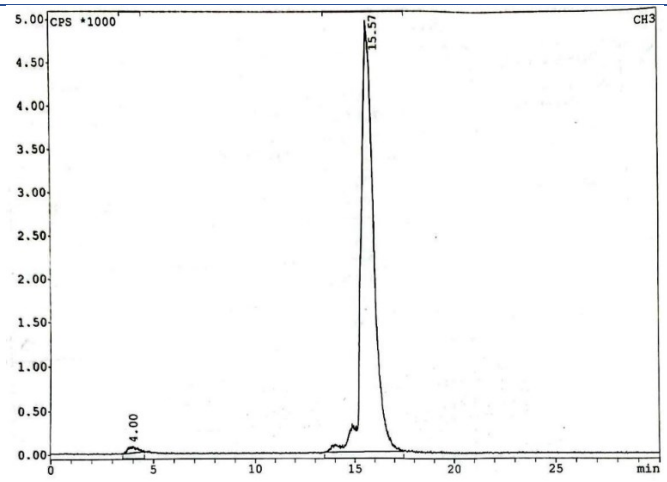


**Figure 2**. HPLC chromatogram of [$^{113m}$In]In-AMBA

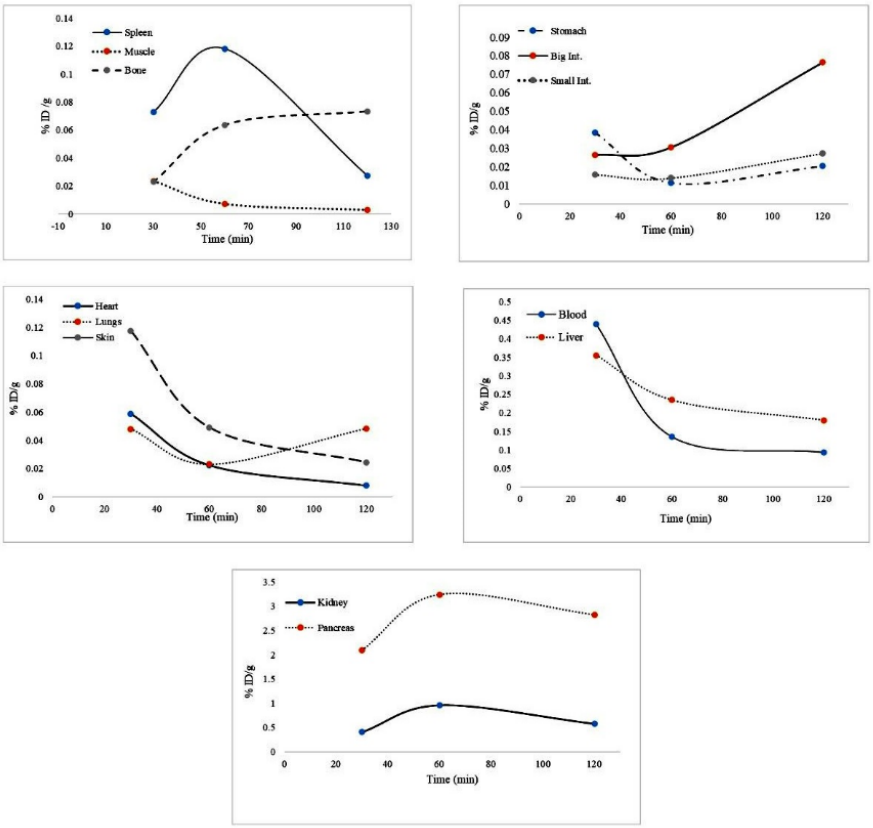


**Figure 3.** Non-decay corrected curve of [$^{113m}$In]In-AMBA at various time points in rats

### *Estimation of human absorbed dose*

Monte Carlo simulations were conducted using the ORNL adult male human phantom to calculate the SAFs and S-values for the $^{113m}$In radionuclide. The analysis of SAFs from this study showed a discrepancy of less than 5% when compared to the values obtained from the OLINDA software, confirming the accuracy of the simulation. Table 1 shows the comparison of SAF values obtained from our MCNPX-based Monte Carlo simulation and the standard OLINDA/EXM software for several key human organs.

The S-values for the $^{113m}$In radionuclide were determined using the human ORNL phantom. In conclusion, the absorbed dose for humans following the injection of [$^{113m}$In]In-AMBA was estimated based on biodistribution data derived from the animal model (Table 2).

**Table 1.** Comparison of SAF values (MeV/g) for selected human target organs, using the kidneys as the source organ, at photon energy of 0.2 MeV. SAFs were calculated using MCNPX Monte Carlo simulations based on the ORNL adult male phantom and F6 tally

| Source Organ | Target Organ | OLINDA | MCNP2.6 | Error (%) |
|---|---|---|---|---|
| Kidneys | LLI Wall | 2.05829E-05 | 2.16E-05 | 4.82 |
| Kidneys | Small Intestine | 1.23733E-05 | 1.21E-05 | 2.17 |
| Kidneys | Stomach | 1.03766E-05 | 1.06E-05 | 2.48 |
| Kidneys | ULI Wall | 1.39078E-05 | 1.33E-05 | 4.53 |
| Kidneys | Heart Wall | 3.94989E-06 | 3.81E-06 | 3.66 |
| Kidneys | Kidneys | 0.000251295 | 0.000254 | 1.11 |
| Kidneys | Liver | 1.92329E-05 | 1.95E-05 | 1.23 |
| Kidneys | Lungs | 3.43478E-06 | 3.31E-06 | 3.7 |
| Kidneys | Spleen | 3.86221E-05 | 3.77E-05 | 2.45 |

**Table 2.** Estimation of the human absorbed dose after the injection of [$^{113m}$In]In-AMBA

| Organ name | Absorbed dose (mGy/37 MBq) | Organ name | Absorbed dose (mGy/37 MBq) |
|---|---|---|---|
| Gallbladder | 0.0288±0.0021 | ULI wall | 0.0148±0.0009 |
| Brain | 0.0041±0.0006 | Bone surface | 0.0155±0.0011 |
| Adrenals | 0.0344±0.0026 | Kidneys | 0.0667±0.0037 |
| LLI Wall | 0.0073±0.0008 | Thymus | 0.0078±0.0005 |
| Small Intestine | 0.0126±0.0013 | Lungs | 0.0122±0.0087 |
| Stomach | 0.0219±0.0015 | Muscle | 0.0089±0.0008 |
| Pancreas | 0.1634±0.0114 | Heart wall | 0.0163±0.0011 |
| Red marrow | 0.0156±0.0013 | Skin | 0.0049±0.0091 |
| Spleen | 0.0305±0.0046 | Liver | 0.0323±0.0009 |
| Total Body | 0.0128±0.0022 | Urine bladder | 0.0051±0.0006 |

## DISCUSSION

In this study, the absorbed dose of [$^{113m}$In]In-AMBA in humans was estimated using the MIRD methodology. According to the FDA and EANM, preclinical dosimetry an essential step in the development of novel radiopharmaceutical agents. Preclinical dosimetry allows researchers to understand the in vivo behavior of radiolabeled compounds under various conditions and investigate potential side effects [15]. Therefore, [$^{113m}$In]In-AMBA was prepared and its biodistribution was assessed. Finally, the absorbed dose in humans was estimated based on biodistribution data obtained from rats using MCNP simulating code. While OLINDA/EXM

remains a widely accepted tool for internal dose assessment, its reliance on stylized phantoms and fixed SAF libraries may limit its application in novel radiopharmaceutical modeling. In contrast, Monte Carlo-based simulation using MCNPX 2.6.0 offers direct control over source geometry, energy spectra, and organ-specific interaction, as supported by previous literature, making it a more adaptable and precise approach for evaluating emerging agents.

A comparison of organ-absorbed doses revealed that the highest doses were observed in the pancreas (0.0044±0.0008 mGy/MBq) and kidneys (0.0018±0.0.0004 mGy/MBq). The elevated dose in the pancreas is attributed to the expression of GRPR in this organ, while the high uptake in the kidneys is due to the hydrophilic nature of the radiolabeled compound and its rapid clearance through renal excretion. In contrast, the brain exhibited the lowest absorbed dose among the studied organs (Table 1).

The human absorbed dose of [$^{113m}$In]In-AMBA was compared to that of other structurally similar radiolabeled compounds, as summarized in Table 3. [$^{113m}$In]In-AMBA exhibited consistently lower absorbed dose in all evaluated organs when compared to [$^{111}$In]In-AMBA. This difference is primarily due to the shorter half-life of $^{113m}$In compared to $^{111}$In (Table 4). Additionally, $^{18}$F-BAY 864367 (a BBN analog) showed a higher absorbed dose than [$^{113m}$In]In-AMBA, which can be attributed to the monoenergetic nature and shorter half-life of $^{113m}$In. The absorbed doses reported in this study were found to be substantially lower than organ-specific safety thresholds reported in the literature. For instance, the pancreatic dose of 0.0044 mGy/MBq remains well within the diagnostic reference range and is considerably lower than doses reported for [$^{111}$In]In-AMBA and $^{18}$F-BAY 864367, supporting the safety of [$^{113m}$In]In-AMBA for clinical use. Moreover, the chemistry of $^{113m}$In is simpler than that of $^{99m}$Tc for labeling purposes [14, 31]. $^{113m}$In can be easily in the form of high half-life $^{113}$Sn/$^{113m}$In generator, which addresses the shortage of $^{99}$Mo. Therefore, owing to its favorable characteristics, including straightforward radiolabeling, low organ-absorbed doses, and suitable imaging properties, [$^{113m}$In]In-AMBA is a suitable candidate for SPECT imaging in the body.

**Table 3.** Comparison of the human absorbed dose (mGy/MBq) for $^{111}$In-AMBA, $^{18}$F-BAY 864367, $^{l11}$In DTPA-D-Phe OCTREOTIDE and [$^{113m}$In] In-AMBA

| | $^{113m}$In-AMBA | $^{111}$In-AMBA | $^{18}$F-BAY 864367 | $^{l11}$In DTPA-D-Phe OCTREOTIDE |
|---|---|---|---|---|
| **Heart** | 0.0004 | 0.072 | 0.0134 | - |
| **Kidneys** | 0.0018 | 0.12 | 0.0166 | 0.31 |
| **Liver** | 0.0009 | 0.2 | 0.0221 | 0.09 |
| **Lungs** | 0.0003 | 0.074 | 0.0096 | 0.02 |
| **Bone** | 0.0004 | 0.22 | 0.0176 | 0.03 |
| **Muscle** | 0.0002 | 0.07 | 0.0084 | 0.02 |
| **Small Intestine** | 0.0003 | 0.11 | 0.0149 | 0.04 |
| **Pancreases** | 0.0044 | 0.25 | 0.0144 | 0.06 |
| **Spleen** | 0.0008 | 0.12 | 0.0101 | 0.44 |
| **References** | This study | [32] | [33] | [34] |

**Table 4.** Comparison of physical properties of some diagnostic radionuclides [35]

| | $^{18}$F | $^{111}$In | $^{113m}$In |
|---|---|---|---|
| **Half-Life** | 110 min | 2.8 day | 99 min |
| **Decay mode** | β+ | EC | IT |
| **Eβ+ (keV)** | 249.8 (96.73 %) | - | - |
| **Eγ (keV)** | - | 245.35 (94.1)<br>171.28 (90.7) | 391.698(64.94%) |

β+: Positron decay, EC: Electron capture, IT: Isomeric transition

The substantial difference in absorbed dose estimates between [$^{111}$In]In-AMBA and [$^{113m}$In]In-AMBA primarily arises from the distinct physical properties of the two radionuclides. As shown in Table 4, $^{111}$In has a significantly longer half-life (2.8 days) compared to $^{113m}$In (99 min), which directly impacts the time-integrated activity (Ã) in organs. The longer residence time of $^{111}$In in tissues leads to higher cumulative radiation exposure and therefore higher absorbed doses.

Additionally, $^{111}$In emits two prominent gamma photons at 245 and 171 keV with high emission probabilities (~94% and ~91%, respectively), whereas $^{113m}$In emits a single gamma photon at 391.7 keV with a lower emission probability (~65%). This difference affects both the energy deposition and photon interactions within tissues, further contributing to the dose discrepancy.

Furthermore, the shorter half-life of $^{113m}$In limits the duration of radiation exposure, which results in significantly lower absorbed doses across all organs. Despite this, $^{113m}$In still provides adequate imaging performance within its optimal time window post-injection. Therefore, the lower absorbed dose associated with [$^{113m}$In]In-AMBA is consistent with its physical characteristics and supports its suitability for safe diagnostic applications.

Despite the promising dosimetric and biochemical characteristics of [$^{113m}$In]In-AMBA, practical challenges arise due to the relatively short physical half-life of $^{113m}$In (99 min). This short half-life necessitates the availability of on-site or nearby isotope generators to ensure timely and continuous production of the radiotracer. Advances in the design and construction of $^{113}$Sn/$^{113m}$In generator systems have demonstrated the capability to produce high-purity $^{113m}$In with satisfactory yield and stability. These developments effectively mitigate the limitations posed by the short half-life and facilitate the clinical application of $^{113m}$In-labeled radiopharmaceuticals. Thus, while operational challenges exist, ongoing technological improvements in generator systems support the practical use of $^{113m}$In in nuclear medicine imaging [13, 36].

Although imaging studies were not included in the current phase due to equipment limitations, future investigations will incorporate micro-SPECT/CT imaging to directly assess tumor targeting, image quality, and diagnostic accuracy of [$^{113m}$In]In-AMBA. These studies will complement the current dosimetry findings and further validate the clinical potential of this radiopharmaceutical. Future studies incorporating in vivo imaging and tumor-bearing models will be critical to confirm the diagnostic performance of this promising GRPR-targeted radioligand.

## CONCLUSION

In this study, [$^{113m}$In]In-AMBA was successfully prepared with high radiochemical purity (>98%). Biodistribution studies in rats demonstrated high uptake in GRPR-expressing organs such as the pancreas, with rapid clearance from non-target tissues. Monte Carlo simulations based on the MIRD schema and ORNL phantom were employed to estimate human absorbed doses using preclinical data. The pancreas and kidneys received the highest doses (0.0044 and 0.0018 mGy/MBq, respectively), while all other organs received low doses within the safe diagnostic range. These features, combined with simple labeling chemistry and availability via $^{113}$Sn/$^{113m}$In generators, make it a promising SPECT radiotracer for imaging GRPR-positive tumors. Further studies involving imaging in tumor-bearing models and early-phase clinical trials are warranted to fully validate the safety, efficacy, and diagnostic performance of [$^{113m}$In]In-AMBA.

## REFERENCES

1. Morgat C, MacGrogan G, Brouste V, Vélasco V, Sévenet N, Bonnefoi H, Fernandez P, Debled M, Hindié E. Expression of gastrin-releasing peptide receptor in breast cancer and its association with pathologic, biologic, and clinical parameters: a study of 1,432 primary tumors. J Nucl Med. 2017 Sep;58(9):1401-7 .
2. Ma Y, Gao F. Advances of radiolabeled GRPR ligands for PET/CT imaging of cancers. Cancer Imaging. 2024 Jan 26;24(1):19 .
3. Cornelio DB, Roesler R, Schwartsmann G. Gastrin-releasing peptide receptor as a molecular target in experimental anticancer therapy. Ann Oncol. 2007 Sep;18(9):1457-66 .
4. Pu F, Xue S, Yang JJ. ProCA1.GRPR: a new imaging agent in cancer detection. Biomark Med. 2016 May;10(5):449-52 .
5. Baratto L, Duan H, Mäcke H, Iagaru A. Imaging the distribution of gastrin-releasing peptide receptors in cancer. J Nucl Med. 2020 Jun;61(6):792-8 .
6. Bratanovic IJ, Zhang C, Zhang Z, Kuo HT, Colpo N, Zeisler J, Merkens H, Uribe C, Lin KS, Bénard F. A radiotracer for molecular imaging and therapy of gastrin-releasing peptide receptor-positive prostate cancer. J Nucl Med. 2022 Mar;63(3):424-30 .
7. Dalm SU, Bakker IL, de Blois E, Doeswijk GN, Konijnenberg MW, Orlandi F, Barbato D, Tedesco M, Maina T, Nock BA, de Jong M. 68Ga/177Lu-NeoBOMB1, a novel radiolabeled GRPR antagonist for theranostic use in oncology. J Nucl Med. 2017 Feb 1;58(2):293-9.
8. Accardo A, Galli F, Mansi R, Del Pozzo L, Aurilio M, Morisco A, Ringhieri P, Signore A, Morelli G, Aloj L. Pre-clinical evaluation of eight DOTA coupled gastrin-releasing peptide receptor (GRP-R) ligands for in vivo targeting of

receptor-expressing tumors. EJNMMI Res. 2016 Dec;6(1):17 .

9. Baum R, Prasad V, Mutloka N, Frischknecht M, Maecke H, Reubi MJ. Molecular imaging of bombesin receptors in various tumors by Ga-68 AMBA PET/CT: first results. J Nucl Med. 2007 May;48(Supplement 2):79P.
10. Fox J, Maddalena ME, Wedeking P, Chen J, Wang N, Linder K, Nunn A, Lantry L. Comparative biodistributions of 111In, 67Ga and 177Lu-AMBA in PC-3 tumor bearing mice. J Nucl Med. 2007 May;48(Supplement 2):79P
11. Ho CL, Liu IH, Chen LC, Lee WC, Wu YH, Chen CL, Jan ML, Lin WJ, Lee TW, Chang CH. Receptor binding assay, biodistribution and micro-SPECT/CT imaging of 111In-AMBA in human prostate tumor-bearing mice. J Nucl Med. 2010 May;51(2):1524
12. Dewanjee MK. The chemistry of 99mTc-labeled radiopharmaceuticals. Semin Nucl Med. 1990 Jan;20(1):5-27.
13. Bolorinovin, F., Mirzaei, M., Faghihi, R., Joharidaha, F., Sina, S., Hadad, K., Yousefnia, H. Design and construction of a 113Sn/113mIn generator using irradiation of natural indium in a cyclotron accelerator. J Nucl Sci Eng Technol. 2024; 45(1): 99-106 .
14. Akbari L, Sina S, Zolghadri S, Moghaddasi A, Hadad K, Yousefnia H. [113mIn]In-PSMA: high potential agent for SPECT imaging of prostate cancer. Radiochim Acta. 2024 Nov 26;112(11):883-94.
15. Stokke C, Gnesin S, Tran-Gia J, Cicone F, Holm S, Cremonesi M, Blakkisrud J, Wendler T, Gillings N, Herrmann K, Mottaghy FM, Gear J. EANM guidance document: dosimetry for first-in-human studies and early phase clinical trials. Eur J Nucl Med Mol Imaging. 2024 Apr;51(5):1268-86.
16. Yousefnia H, Zolghadri S, Jalilian AR, Tajik M, Ghannadi-Maragheh M. Preliminary dosimetric evaluation of (166)Ho-TTHMP for human based on biodistribution data in rats. Appl Radiat Isot. 2014 Dec;94:260-5.
17. Radfar E, Jalilian AR, Yousefnia H, Bahrami-Samani A, Ghannadi-Maragheh M. A comparative study of preliminary dosimetry for human based on distribution data in rats with 111In, 90Y, 153Sm, and 177Lu labeled rituximab. Nucl Technol Radiat Prot. 201;27(2):144-51.
18. Stabin MG, Siegel JA. Physical models and dose factors for use in internal dose assessment. Health Phys. 2003 Sep;85(3):294-310.
19. Ocampo JC, Puerta JA, Morales J. Evaluation of specific absorbed fractions from internal photon sources in the ICRP Reference Male Phantom. Radiat Prot Dosimetry. 2013 Nov;157(1):133-41.
20. Luo XY, Qiu R, Wu Z, Yan SC, Hu ZY, Zhang H, Li JL. THUDose PD: a three-dimensional Monte Carlo platform for phantom dose assessment. Nucl Sci Tech. 2023 Nov;34(11):164.
21. Subramanian S, He B, Frey E, Jokisch DW, Bolch W, Sgouros G. Improved accuracy of S-value-based dosimetry: a guide to transition from Cristy-Eckerman to ICRP adult phantoms. EJNMMI Phys. 2022 Aug 26;9(1):57 .
22. Zolghadri S, Bakhshi Kashi M, Vahidfar N, Farzanefar S, Karimian A, Mohammadi Ashnani MH, Yousefnia H. First-in-human dosimetry and safety evaluation of 68Ga-αMSH derivative for PET imaging of melanoma. Sci Rep. 2025 May 22;15(1):17748 .
23. Han EY, Bolch WE, Eckerman KF. Revisions to the ORNL series of adult and pediatric computational phantoms for use with the MIRD schema. Health Phys. 2006 Apr;90(4):337-56 .
24. Wang W, Cheng MY, Long PC, Hu LQ. Specific absorbed fractions of electrons and photons for Rad-HUMAN phantom using Monte Carlo method. Chin Phys C. 2015 Jul;39(7):078203.
25. Karimkhani S, Yousefnia H, Faghihi R, Gramifar P, Parishan MR. Calculation of Gallium-68 dose factors for [68Ga] DOTATATE injected patients: a comparison with OLINDA Database. J Nucl Res Appl. 2022 Jun 1;2(2):30-40.
26. Internal radionuclide dose calculation. [cited 2024 Oct 22]. Available from: https://www.hermesmedical.com/our-software/dosimetry/olinda ⁄
27. Basic anatomical and physiological data for use in radiological protection: reference values. A report of age- and gender-related differences in the anatomical and physiological characteristics of reference individuals. ICRP Publication 89. Ann ICRP. 2002;32(3-4):5-265.
28. Scott JA. Photon, electron, proton and neutron interaction data for body tissues. J Nucl Med. 1993 Jan; 34(1): 171.
29. Hakimabad HM, Motavalli LR. Evaluation of specific absorbed fractions from internal photon sources in ORNL analytical adult phantom. Radiat Prot Dosimetry. 2008;128(4):427-31.
30. Snyder WS, Ford M, Warner G, Watson S. “S” absorbed dose per unit cumulated activity for selected radionuclides and organs. MIRD Pamphlet No. 11. Soc Nucl Med, New York. 1975.
31. Ranjbar S, Aghamiri SM, Rajabifar S, Zolghadri S, Yousefnia H. [113mIn] In-RM2: a high potential agent for SPECT imaging of GRPR-expressing tumors. Phys Eng Sci Med. 2025 Jan 6:1-1.
32. Ho CL, Liu IH, Wu YH, Chen LC, Chen CL, Lee WC, Chuang CH, Lee TW, Lin WJ, Shen LH, Chang CH. Molecular imaging, pharmacokinetics, and dosimetry of In-AMBA in human prostate tumor-bearing mice. J Biomed Biotechnol. 2011;2011:101497.
33. Sah BR, Burger IA, Schibli R, Friebe M, Dinkelborg L, Graham K, Borkowski S, Bacher-Stier C, Valencia R, Srinivasan A, Hany TF, Mu L, Wild PJ, Schaefer NG. Dosimetry and first clinical evaluation of the new 18F-radiolabeled bombesin analogue BAY 864367 in patients with prostate cancer. J Nucl Med. 2015 Mar;56(3):372-8 .
34. Bajc M, Palmer J, Ohlsson T, Edenbrandt L. Distribution and dosimetry of 111In DTPA-D-Phe-octreotide in man assessed by whole body scintigraphy. Acta Radiol. 1994 Jan;35(1):53-7 .
35. Isotope Browser Software. [cited 2024 Oct 22]. Available from: https://play.google.com/store/apps/details?id=iaea.nds.nuclides&hl=en&pli=1
36. Al-Janabi M, Al-Hashimi H. 113m In radioisotope generator system. J Radioanal Nucl Chem. 1979 Mar 1;53(1-2):321-6.